Impact of aerosol hygroscopic growth on retrieving aerosol extinction coefficient profiles from elastic-backscatter lidar signals

Gang Zhao[1], Chunsheng Zhao[1], Ye Kuang[1], Jiangchuan Tao[1], Wangshu Tan[1], Yuxuan Bian[2], Jing Li[1], Chengcai Li[1]

1 Department of Atmospheric and Oceanic Sciences, School of Physics, Peking University, Beijing, China

2 State Key Laboratory of Severe Weather, Chinese Academy of Meteorological Sciences, Beijing, 100081, China

Correspondence to: Chunsheng Zhao (zcs@pku.edu.cn)

Abstract

Light detection and ranging (lidar) measurements have been widely used to profile ambient aerosol extinction coefficient (σ_{ext}). Particle extinction-to-backscatter ratio (lidar ratio, LR), which ~~highly~~ depends on aerosol dry particle number size distribution (PNSD) and aerosol hygroscopicity, is introduced to retrieve the σ_{ext} profile from elastic-backscatter lidar signals. Conventionally, a constant column-integrated LR that is estimated from aerosol optical depth is used by the retrieving algorithms. In this paper, the influences of aerosol PNSD, aerosol hygroscopic growth and relative humidity (RH) profiles on the variation of LR are investigated based on the datasets from field measurements in the North China Plain (NCP). Results show that LR has an enhancement factor of 2.2 when RH reaches 92%. Simulation results indicate that both the magnitude and vertical structures of the σ_{ext} profiles by using column-related LR method are significantly biased from the original σ_{ext} profile. The relative bias, which is mainly influenced by RH and PNSD, can reach up to 40% when RH at the top of the mixed layer is above 90%. A new algorithm for retrieving σ_{ext} profiles and a new scheme of LR enhancement factor by RH in the NCP are proposed in this study. The relative bias between the σ_{ext} profile retrieved with this new algorithm and the ideal true value is reduced to below 13%.

1. Introduction

Atmospheric aerosols can directly scatter and absorb solar radiation, thus exerting significant impacts on the atmospheric environment and climate change. Vertical distributions of aerosol particles are crucial for studying the roles of atmospheric aerosols in the radiation balance of the Earth-Atmosphere system (Kuang et al., 2016), air pollution transportation (Gasteiger et al., 2017) and boundary layer process. However, there remain many problems while determining the spatial and temporal distributions of aerosols because of their highly variable properties (Anderson and Anderson, 2003; Andreae and Crutzen, 1997) and complex sources. As a result, our knowledge about the vertical distributions of aerosols is still very limited.

Light detection and ranging (lidar) instruments are useful remote sensing tools to monitor profiles of aerosol optical properties. This kind of instrument involves a pulsed laser beam, which can be used to detect the back-scatter signals from aerosols and air molecules in the atmosphere (Klett, 1981). Elastic-backscatter lidar is one of the most frequently used instruments (He et al., 2006; Pietruczuk and Podgórski, 2009). However, there are some limitations when deriving aerosol extinction coefficient (σ_{ext}) and aerosol back scattering coefficient (β_{sca}) from elastic-backscatter lidar signals. Many efforts have been carried out to retrieve the σ_{ext} profiles from lidar signals (Klett, 1981, 1985). Particle extinction-to-backscatter ratio, which is usually termed as the lidar ratio (LR), is required when retrieving σ_{ext} profiles (Fernald, 1984; Fernald et al., 1972). LR can be derived directly using Raman lidar (Pappalardo et al., 2004b) and high spectral resolution lidar (She et al., 1992; Shipley et al., 1983; Sroga et al., 1983) measurements. Raman lidar has low signal to noise ratios (SNR) during the day, which may lead to significant bias and uncertainties in retrieving lidar signals. High spectral resolution lidar have high technique requirement and expensive cost. Ansmann et al. (2002) demonstrated that the profile of LR could be retrieved from Raman lidar and this LR profile can be used to retrieve σ_{ext} profiles from high SNR elastic-backscattering lidar data. However, there exist many cases when elastic-backscatter lidar is used without concurrently measured LR profile.

Sun-photometer, radiometer and elastic-backscatter lidar data are usually used simultaneously to retrieve σ_{ext} profiles (Chaikovsky et al., 2016; He et al., 2006). In these studies, σ_{ext} profiles could be retrieved from elastic-backscatter lidar signals by using a constant column-related LR, which is constrained by measurements of aerosol optical depth (AOD) from sun-photometer. However, many factors such as aerosol particle number size distribution (PNSD), aerosol refractive index, aerosol hygroscopicity and ambient relative humidity (RH), have large influences on LR. It is found that the ratio of σ_{ext} and β_{sca} grows linearly but slowly as RH increases when RH is lower than 80% (Ackermann, 1998; Anderson et al., 2000; Ferrare et al., 2001). Further research found that LR is likely to change significantly due to the substantial variation of RH in the mixed layer (Ferrare et al., 1998). Small errors from the initial conditions may lead to large bias of retrieved σ_{ext} profiles (Sušnik et al., 2014). It is likely that using a constant LR profile instead of variable LR profile to retrieve elastic-backscatter lidar data may result in significant bias of retrieved σ_{ext} profiles. The sounding profiles show that RH is highly variable and frequently beyond 80% in the mixed layer in the NCP (Kuang et al., 2016) which is one of the most polluted areas around the world (Ma et al., 2011; Xu et al., 2011). According to this, it is interesting to know how much σ_{ext} profiles retrieved from elastic-backscatter lidar signals will be deviated if constant column-related LR profile is used in the NCP. Few works have been done to assess the bias of using a constant LR profile. This work comprehensively studied the possible bias by employing a large datasets of the field measurements.

To account for the aerosol hygroscopic growth, the κ-K$\ddot{o}$hler theory (Petters and Kreidenweis, 2007) is widely used, in which the chemical composition-dependent variables are merged into a single parameter κ. The κ-K$\ddot{o}$hler equation is expressed as

$$\frac{RH}{100} = \frac{GF^3-1}{GF^3-(1-\kappa)} \cdot \exp\left(\frac{4\sigma_{s/a}M_{water}}{R \cdot T \cdot D_d \cdot gf \cdot \rho_w}\right), \qquad (1)$$

where D_d is the aerosol dry diameter. GF is the aerosol growth factor, which is defined as the ratio of the aerosol diameter under the given RH and dry conditions (D_{RH}/D_d). T is the temperature. $\sigma_{s/a}$ is the surface tension of the solution. M_{water} is the molecular weight of water. R is the universal gas constant and ρ_w is the density of water.

This article is structured in the following way. Section 2 shows all of the data used in this study. Section 3 gives the methodology of this research. Mie theory (Bohren and Huffman, 2007) and κ-K$\ddot{o}$hler theory (Petters and Kreidenweis, 2007) are used to study the influences of aerosol hygroscopic growth on LR. By calculating the LR at different RH, it is found that the RH-related LR profiles are significantly different from the constant LR profile as shown in fig. 1(b). We simulate the bias of the retrieved σ_{ext} profiles by using the AOD related constant LR profiles in three steps. Firstly, the vertical distributions of the aerosol are parameterized and the corresponding aerosol σ_{ext} and β_{sca} profiles are calculated in section 3.2. Secondly, we calculate the theoretical signals received by the elastic-backscatter lidar in section 3.3 by using the σ_{ext} and β_{sca} profiles of the first step. Finally, we retrieve the σ_{ext} profiles from the lidar signals of section 3.3 by using the column related lidar ratio profiles, in which the method is detailed in section 3.4.1. The retrieved σ_{ext} profiles are compared with the parameterized σ_{ext} profiles. In section 3.4.2, we proposed a new method of retrieving the σ_{ext} profiles, which can account for the variations of LR with RH. Results and discussions are shown in section 4. Section 4.2 shows the bias of retrieved σ_{ext} profiles by using a column-related LR profile method. Section 4.2.1 gives the possible bias of the retrieved σ_{ext} profiles and section 4.2.2 shows the sensitivity of the bias under different AOD, different aerosol PNSD, different RH profiles and different aerosol hygroscopicity conditions. In section 4.4, ~~the~~ real-time field measurements ~~results of~~ micro-pulsed lidar (MPL) are used to validate the feasibility of our new proposed method. The conclusions of this research ~~come to the~~ section 5.

2. Data

2.1 Datasets of aerosol properties

During the periods of Haze in China (HaChi) campaign, the physical and chemical properties of aerosol particles ~~are~~ measured at the Wuqing meteorological station. Wuqing ~~site~~ is located between two megacities (Beijing and Tianjin) of NCP, and can represent the pollution conditions of the NCP (Xu et al., 2011).

This study uses the measured datasets of PNSD, black carbon (BC) mass concentrations (Ma et al., 2012) and aerosol hygroscopicity (Chen et al., 2014; Liu et al., 2014) during the field campaign. The sampled aerosol~~s~~ particles are selected to have aerodynamic diameter of less than 10um by an impactor at the initial inlet. These particles are carefully dried to below 40% RH and then led to the corresponding instruments. The aerosol PNSDs with particle diameter in the range from 10nm to 10um are measured by jointly using a differential mobility particle sizer (TDMPS, Leibniz Institute for Tropospheric Research, Germany; Birmili et al., 1999) and an aerodynamic particle sizer (APS,TSI Inc., model 3321) with a temporal resolution of 5 min. The BC mass concentrations are measured by a multi-angle absorption photometer (MAAP model 5012, Thermo, Inc., Waltham, MA USA). The aerosol hygroscopicity is measured by using the humidity tandem differential mobility analyzer (HTDMA), which measures the aerosol GF as a function of RH at different diameter. The aerosol hygroscopicity parameter κ can be directly derived from measurements of HTDMA by applying formula (1).

2.2 RH profiles

The intensive GTS1 observation (Bian et al., 2011) at the meteorological bureau of Beijing (39°48’ N,116°28’ E) were carried out from July to September ~~in~~ 2008. With a resolution of 10m in the vertical direction, the radiosonde data include~~s~~ profiles of temperature, pressure and RH. During the intensive observation period, balloon soundings were performed four times a day.

Water vapor mixing ratio is almost constant in the mixed layer due to extensive turbulent mixing ~~existing~~ and decreases rapidly above the mixed layer. RH profiles that exhibit well-mixed vertical structures are picked out and studied. ~~With this, the maximum RH in the vertical direction can be used as a good representation of RH profiles~~. RH profiles are classified into four typical groups based on the maximum RH ranges: 60%-70%, 70%-80%, 80%-90% and 90%-95% (Kuang et al., 2016). These four kinds of typical well-mixed RH profiles are labeled as P60-70, P70-80, P80-90 and P90-95 respectively. These four kinds of RH profiles, which are shown in fig. 1(a), are used to conduct the sensitivity studies in this article.

2.3 MPL signals

A single wavelength polarization diversity elastic lidar system is installed on the roof of the physics building in Peking University. This instrument is a MPL manufactured by Sigma Space, using a Nd: YVO4 532nm pulsed DC10H-532SS laser source, with a pulse duration of 10.3ns, energy of 6-8uJ and a repetition of 2500Hz. It collects elastically backscattered signals from the atmosphere by separately detecting its parallel and cross polarization components with respect to the polarization of laser. We also used the concurrently measured AOD data from the AERONET BEIJING_PKU station, which is located at the same place as the Lidar.

3. Methodology

3.1 Influences of aerosol hygroscopic growth on LR

3.1.1 Calculate the LR values under different RH conditions

In this ~~research~~, the Mie model (Bohren and Huffman, 2007) is used to study the influence of RH on LR. When running the Mie model, aerosol PNSD, aerosol complex refractive index, black carbon mixing state and black carbon mass concentrations are essential. The results of Mie model contain the information ~~of the~~ σ_{ext} and β_{sca}, which can be used to calculate the LR directly, with $LR = \frac{\sigma_{ext}}{\beta_{sca}}$.

When exposed to ~~the~~ ambient ~~water content,~~ the aerosols ~~get hygroscopic growth~~. To account for this, the size-resolved hygroscopicity parameter κ, which is derived from the measurements of HTDMA (Chen et al., 2012; Liu et al., 2011)~~, is used in this study~~. ~~The used~~ size-resolved κ is shown in fig. S1. Mean value of size-resolved κ during the Hachi Campaign is used. With this, the aerosol GF ~~of~~ different ~~size at different~~ RH can be calculated by applying formula (1).

Mixing states of BC come from the measurement during the Hachi Campaign. In previous work, BC mixing states during the Hachi campaign were presented as both core-shell mixed and externally mixed (Ma et al., 2012). Ma et al. (2012) provides the ratio of BC mass concentration under externally mixed state to total BC mass concentration as follows:

$$r_{ext\_BC} = \frac{M_{ext\_BC}}{M_{BC}} \qquad (2).$$

M_{ext_BC} is the mass concentration that is externally mixed and M_{BC} is the total mass concentration of BC. The mean value of r_{ext_BC}=0.51 (Ma et al., 2012) is used as a representation of the mixing state in this study. The size-resolved distribution of BC mass concentration is the same as that used by Ma et al (2012a).

The refractive index ($\tilde{m}$), with accounting for the water content in the particle, is derived as a volume mixture between the dry aerosol and water (Wex et al., 2002):

$$\tilde{m} = f_{V,dry}\, \tilde{m}_{aero,dry} + (1 - f_{V,dry})\, \tilde{m}_{water} \qquad (3).$$

$f_{v,dry}$ is the ratio of the dry aerosol volume to total aerosol volume at given RH condition; $\tilde{m}_{aero,dry}$ is the refractive index of dry ambient aerosols and $\tilde{m}_{water}$ is the refractive index of water content absorbed by aerosols. The refractive indices of BC, non-light-absorbing aerosols and water, which are used in this study, are 1.8+0.54i (Kuang et al., 2015), 1.53+10^{-7}i (Wex et al., 2002) and 1.33+10^{-7} respectively.

To sum up, we can calculate the LR of a PNSD under the given RH condition by using the Mie scattering model. For a dry aerosol PNSD, the corresponding aerosol PNSD at a given RH can be calculated by applying the size resolved κ and formula (1). Aerosol refractive index can be determined from formula (3), too. With this information, LR can be calculated. For each aerosol PNSD, we change the RH from 40% to 95% to calculate the LR values at different RH. Finally, the LR values of different measured aerosol PNSD at different RH are calculated by using the same method.

3.1.2 Parameterizing the variation of LR with RH

When the LR values under different RH are statistically studied, we find that the LR can be enhanced when the RH increases, which will be discussed in detail in section 4.1.1 and fig 2.

The LR enhancement factor is introduced to describe the influence of aerosol hygroscopic growth on LR at different RH. It is defined as the ratio of LR at a given RH to LR at the condition of RH<40%. We give the statistically mean relationships between the LR enhancement factor and RH. The LR enhancement factor can account for the incensement of LR with RH and the parameterized LR enhancement factor is further used in our proposed method to retrieve the σ_{ext} profiles.

3.2 LR profiles and σ_{ext} profiles

~~Assumptions about aerosol properties in the vertical direction are made to calculate LR profiles and σ_{ext} profiles.~~

Liu et al. (2009) studied vertical profiles of aerosol total number concentration (Na) with aircraft measurements. ~~Vertical distributions of Na are parameterized according to the vertical distribution properties of Na. Results showed that~~ Na is ~~relatively~~ constant in the mixed layer. A transition layer where ~~Na~~ linearly decreases ~~exists in the parameterized scheme. Na also~~ exponentially decreases above the transition layer. The same parameterized scheme proposed by Liu et al. (2009) is adopted by this study. Both the study of Liu et al. (2009) and Ferrero et al. (2010) manifests that the dry aerosol PNSD in the mixed layer varies little. The shape of dry aerosol PNSD is assumed constant ~~along~~ with ~~the~~ height, which means that aerosol PNSD at different heights divided by Na give the same normalized PNSD.

As for the BC vertical distribution, Ferrero et al. (2011) and Ran et al. (2016) demonstrate that BC mass concentration in the mixed layer remains relatively constant and decreases sharply above the mixed layer. According to this, parameterization scheme of BC vertical distributions is assumed the same as that of ~~the~~ aerosol. The shape of the size-resolved BC mass concentration distribution is also assumed the same as that at the surface.

LR profiles and σ_{ext} profiles can be calculated by Mie theory under these assumptions. Details of computing σ_{ext} profiles can be found at Kuang et al. (2015). The calculated LR profiles and σ_{ext} profiles are used in the following study to provide the theoretical elastic-backscatter signals.

3.3 Simulated elastic-backscatter lidar signals

The intensity of signals received by elastic-backscatter lidar depends on optical properties of objects and the distance between scattering objects and receiving system. It can be typically described by the following formula:

$$P(R) = C \times P_0 \times \frac{\beta(R)}{R^2} \times e^{\int_0^R -2\times\sigma(r)\times dr} \qquad (4).$$

In formula (4), P_0 is the intensity of the laser pulse. R is the spatial distance between scattering objects and the receiving system. C is a correction factor determined by the status of elastic-backscatter lidar machine itself. β(R) refers to the sum of aerosol backscattering coefficient

(β_{sca}) and air molecule backscattering coefficient ($\beta_{sca,mole}$) at distance R. $\sigma(R)$ denotes the sum of σ_{ext} and air molecule's extinction coefficient ($\sigma_{ext,mole}$). $\beta_{sca,mole}$ and $\sigma_{ext,mole}$ can be calculated by using Rayleigh scattering theory when the temperature and pressure are available.

In this study, we can theoretically get the intensities of elastic-backscatter lidar signals and the AOD from each given σ_{ext} and β_{sca} profiles with the assumption that C is equal to one. Retrieving elastic-backscatter lidar signals can result in exactly the same σ_{ext} profile as the original one when the profile of LR is available. However, a constant column-related LR profile is used to retrieve elastic-backscatter lidar signals and the retrieved σ_{ext} profile would deviate from the given σ_{ext} profile when there is insufficient information about the LR profile.

3.4 Retrieving σ_{ext} profiles from elastic-backscatter lidar signals

3.4.1 Retrieving σ_{ext} profiles by using constant column-related LR profile method

Traditionally, the AOD from sun-photometer and the elastic-backscatter lidar signals are combined to retrieve the σ_{ext} profiles. Additional information is needed to get the mathematical results of formula (4) because there are two unknown parameters (β_{sca} and σ_{ext}). The commonly used method of solving this formula is to assume a constant value of column-related LR and then the profiles of σ_{ext} and β_{ext} can be retrieved (Fernald, 1984; Klett, 1985). Different values of column-related LR can lead to different σ_{ext} profiles and different AOD. A constant column-related LR can be constrained if sun photometer is concurrently measuring the AOD (He et al., 2006; Pietruczuk and Podgorski, 2009). Thus, σ_{ext} profile can be retrieved by using the column-related constant LR profile.

3.4.2 Retrieving σ_{ext} profiles accounting for aerosol hygroscopic growth

A new method of retrieving σ_{ext} profiles from elastic-backscatter lidar signals is proposed, in which the variation of LR with RH can be taken into consideration. This new method requires the measured elastic-backscatter lidar signals, measured AOD data and RH profiles.

A schematic diagram of this method is shown in Fig.2. A parameterized LR profile is used to retrieve σ_{ext} profiles instead of an AOD-constrained constant LR profile. Firstly, the LR enhancement factor are statistically studied and parameterized under different polluted conditions. The results of mean parameterized LR enhancement factor, which is detailed in section 4.1.1, are used in this study. LR profile can be calculated by using RH profile, a LR value at dry state and the equations of LR enhancement factor. σ_{ext} profile can be retrieved with combination of LR profile and formula (4). Dry state LR value can be constrained by comparing the integrated AOD value of retrieved σ_{ext} profile and concurrently measured AOD value. LR profile is determined and σ_{ext} profile can be retrieved with the constrained dry state LR.

4. Results and Discussion

4.1 LR properties

4.1.1 Variation of LR with RH

During the field campaign of Hachi, there is a total 3540 different aerosol PNSDs. These aerosol PNSDs can be used as a good representation datasets of the continental aerosol. LR is calculated by using different aerosol PNSD and RH values between 30% and 95%.

Relationships between dry state LR and concurrently measured σ_{ext} (sum of the aerosol scattering and absorption) are shown in Fig. 2(a). It shows that LR can vary across a wide range from 30 sr to 90 sr, which is consistent with the literature values of continent aerosols (Ansmann et al., 2001; Pappalardo et al., 2004a). This also indicates that calculating the LR by using Mie theory is feasible. Fig. 2(b) gives the probability distribution function of the LR. Most of the LR lies in the range between 45~65 sr.

By calculating the LR values under different RH, we find that the LR tends to increase with RH. Relationships between the LR enhancement factor and RH are given in Fig. 2(c). The LR enhancement factor has a mean value lower than 1.2 when the RH is lower than 70%. LR increases linearly with RH when RH is lower than 80%, which is consistent with the literal results (Salemink et al., 1984). However, LR can be enhanced by a factor of 2.2 when the RH reaches 92% with mean hygroscopicity of aerosol.

Mean values of LR enhancement factor are parameterized as below:

$$RH_0 = \mathrm{RH} - 40 \qquad (5)$$

$$\mathrm{LR} = LR_{dry} \times (0.92 + 2.5 \times 10^{-2} RH_0 - 1.3 \times 10^{-4} RH_0^2 + 2.2 \times 10^{-5} RH_0^3) \qquad (6).$$

This parameterization equation can be used as a representation of the mean effect of continental aerosol hygroscopicity on LR.

The incensement of LR with RH has been studied before. Ackermann (1998) calculates the relationships of LR with RH by using the lognormal distribution of aerosols as the input of Mie scattering theory and finds that the LR increases with RH for the continental aerosols. However, Ackermann (1998) shows that the LR doesn't show the same properties for maritime aerosols and desert aerosols.

We theoretically analyze the reasons of ~~the~~ LR by using the Mie scattering model and the mean aerosol PNSD of the Hachi campaign. By definition, LR is the ratio of σ_{ext} to β_{sca}. β_{sca} can be written as $\beta_{sca} = \frac{\sigma_{ext}\times SSA\times PF(180)}{4\times\pi}$, where the SSA is single scattering albedo, which is defined as the ratio of extinction coefficient and scattering coefficient. PF(180) is the aerosol scattering phase function at the scattering angle of 180^{o}. Thus, $\mathrm{LR} = \frac{\sigma_{ext}\times 4\times\pi}{\sigma_{ext}\times SSA\times PF(180)} = \frac{4\times\pi}{SSA\times PF(180)}$. We use the mean aerosol PNSD as the input of Mie scattering model and calculate the aerosol phase function and SSA values at different RH. When particle grows, there tends to be larger partition of forward scattering and PF(180) is smaller, which is shown in fig.S2. The PF(180) decreases 40% from 0.27 to 0.16. At the same time, the SSA increases 5% from 0.93 to 0.97 and PF(180) as shown in fig.S3. Thus, the LR increases with the ~~incensement~~ of RH.

4.1.2 LR ratio profiles

Four different types of RH profiles and LR profiles are shown in fig 1. In Fig. 1(a), RH values increase with height in the mixed layer and decrease with height above the mixed layer. This is a synthetic result of temperature and water content distributions in the vertical direction. In the summer afternoon, water vapor is well mixed within the mixed layer and decreases sharply above the mixed ~~layer~~. P60-70 can represent the relatively dry environmental conditions. Statistical results show that P80-90 is most likely to be observed in the environment. P90-95 is a very moist environment condition and its frequency of being observed is second to that of the P80-90 type.

Profiles of LR corresponding to RH profiles of the left column are shown in Fig. 1(b). For each type of LR profile, LR increases with height in the mixed layer due to the increase of RH. At the ground, the mean values of LR for each RH profiles are 38.19, 38.28, 39.53 and 40.33 sr, with a standard deviation of 6.20, 6.22, 6.42 and 6.45 respectively. LR changes little from 38 sr at the ground to 42 sr at the top of the mixed layer when the ambient RH is low for the RH profile of P60-70. However, LR grows with a mean value from 40 sr to 60 sr with a relative difference of 50% when the RH is high for the RH profile of P90-95. With such high variation of LR with RH, the retrieved σ_{ext} profiles might be ~~greatly deviated~~ when using a constant LR profile instead of a variable one.

The black dotted line in Fig. 1(b) is one of the constant column-related LR profiles that are used as an input ~~of~~ retrieving σ_{ext} profiles related to the RH profile P70-80. The constant LR has a higher value at the ground and a lower value at the top of the mixed layer when compared with the calculated variable LR profiles.

During the Hachi Campaign, LR values that are calculated by using Mie theory can change from 30 to 55 sr within 12 hours at the ground (about 87% of initial value). With high variation of LR over time, the LR profile should be updated in time to get an accurately retrieved σ_{ext} profile. Using only one measurement of LR profile to retrieve the σ_{ext} profiles may lead to great bias of retrieved results (Rosati et al., 2016).

4.2 Bias of retrieved σ_{ext} profiles

With the parameterized σ_{ext} profiles by using the method of section 3.2, we can theoretically get the AOD and the elastic-backscatter lidar signals. Then the AOD and the elastic-backscatter lidar signals can be used to constrain a column-related constant LR profile and to retrieve σ_{ext} profiles. Finally, the retrieved σ_{ext} profiles are compared with the parameterized σ_{ext} profiles and the differences are statistically studied.

4.2.1 Retrieved σ_{ext} profiles vs. original σ_{ext} profiles

Fig. 4 provides an example of the retrieved σ_{ext} profile by using the variable LR profile method and that by using the constant LR profile method from simulated lidar signals. These two kinds of profiles can also be described as a given parameterized σ_{ext} profile and a retrieved σ_{ext} profile from constant LR profile. In Fig. 4(a), the retrieved σ_{ext} profile by using a variable LR profile method is demonstrated by solid line. Dotted line shows the retrieved σ_{ext} profile by using a constant column related LR method. Fig. 4(b) shows the relative bias of the two retrieved σ_{ext} profiles at each height. Fig. 4(c) and (d) are almost the same as Fig. 4(a) and (b) respectively, except that the results of Fig. 4(a) and (b) come from the RH profile of P70-80 while those of Fig. 4(c) and (d) come from the RH profile of P90-95.

It is shown in Fig. 4(a) that the retrieved σ_{ext} by using a variable LR profile method increases with height at a rate of 92.25 ($Mm^{-1}km^{-1}$) in the mixed layer, which is consistent with the aerosol loading and RH distribution. However, the retrieved σ_{ext} profile by using a constant LR profile method behaves differently and decreases at a rate of -152.87 ($Mm^{-1}km^{-1}$). The structure of σ_{ext} profiles is different by using two different methods. Moreover, the retrieved σ_{ext} from RH profile of P90-95 at the top of the mixed layer is significantly deviated with a relative bias of 40%.

Both Fig. 4(a) and (c) show that the retrieved σ_{ext} is overestimated at ground and underestimated at the top of the mixed layer. From Fig 3(b), it can be concluded that the AOD-constrained constant LR is larger than the calculated true LR at the ground and smaller at the top of the mixed layer. According to formula (3), signals of the elastic-backscatter lidar received at any height are proportional to the backscattering capability of the aerosols. When LR is larger, a larger fraction of the signals transfer forward and less is scattered back. In order to receive the same amount of signal, the backscattering coefficient should be larger and this can lead to the result of a larger σ_{ext} at that layer. Thus, the σ_{ext} tends to be biased higher than the given parameterized σ_{ext} when the LR is larger, and vice versa. Overall, the profiles retrieved by using an AOD-constrained LR can lead to a positive bias at the ground and a negative bias at the top of mixed layer.

4.2.2 Sensitivity Study

Simulations are conducted to study the characteristics of the retrieved σ_{ext} profile bias between using the constant column-related LR profile and variable LR profile. Different kinds of aerosol PNSD, AOD, aerosol hygroscopicity and RH profiles are used. Aerosol PNSD data comes from the Hachi Campaign field measurement. The sensitivity of the bias in aerosol hygroscopicity is evaluated by changing the size-resolved κ value. Aerosols are defined to have high hygroscopicity when the aerosol size-resolved κ value is one standard deviation above the mean of the size-resolved κ value. They are defined as low hygroscopicity if the size-resolved κ value is one standard deviation below mean of the size-resolved κ value. Four different kinds of RH profiles are also used in this sensitivity study. As discussed in section 3.2.1, a negative bias at the top of the mixed layer is accompanied by a positive bias at the ground and the largest bias happens at the top of the mixed layer. It is sufficient to focus on the relative bias at the top of the mixed layer.

Statistical characteristics of the relative bias at the top of the mixed layer are shown in Fig. 5. Different panels represent the results of different aerosol hygroscopicity. The left column shows the results of low aerosol hygroscopicity. Middle panel shows results from mean aerosol hygroscopicity. High aerosol hygroscopicity of particles results in the properties shown in the right panel. For each panel, relationships between relative bias and AOD are shown. Different colors in each panel show the results of different RH profiles. Filled colors represent the ranges of the relative bias at one standard deviation of using different PNSD.

Every panel show that relative bias clearly increases with the enhancement of RH in the surroundings. The relative bias has a mean value of less than 10% for RH profile of P60-70. LR has little variation when the surrounding RH is low and the bias has a low value. For RH profiles of P70-80 and P80-90, the relative bias increases with RH and increases strongly up to 25% when the surrounding relative humidity is high. These behaviors of relative difference under difference RH conditions are consistent with the change of LR with RH.

Filled color ranges of relative bias at given AOD and RH profile result from the variation of aerosol PNSD. The LR enhancement factor can have different behavior with different aerosol PNSD according to Mie scattering theory. Changing the aerosol PNSD leads to a wider range of bias when the RH is higher. Fig. 5 also shows that different PNSD can change the relative bias by a mean value of 10% for different polluted conditions.

Relative bias increases with AOD value when the AOD is low, while it remains constant when the AOD is high. When AOD is low, the amount of scattered light by air molecules occupies a large fraction. Air molecules have a constant LR of $\frac{8}{3}\pi$ sr according the Rayleigh scattering theory. The relative bias of retrieved σ_{ext} profile is relatively small when the AOD is low. When the AOD has a larger value, backscattered signals mainly depend on aerosol backscattering and the signals backscattered by air molecules are negligible. Relative bias mainly reflects the impacts of aerosol hygroscopicity. The mean relative bias increases from 26% to 32% at high RH conditions with the increase of aerosol hygroscopicity. Aerosol hygroscopicity should be taken into account under high RH conditions.

To sum up, RH is one of the most important factors that influence the accuracy of retrieving the elastic-backscatter lidar data. Different PNSD can also lead to a large variation of relative difference. The relative difference increases with the AOD when the AOD is low, but increases little when the AOD is high. Under the conditions of both high values of RH and AOD, the relative bias of retrieved data reaches a maximum due to the influence of aerosol hygroscopic growth.

4.3 Evaluation of LR enhancement factor parameterization

Simulations are carried out to test the accuracy of the new methods of retrieving the σ_{ext} profiles, which is proposed in section 3.4.2. These simulations employ the elastic-backscattering lidar signals from section 3.3, the RH profiles, the integrated AOD values of the parameterized σ_{ext} profiles and the parameterization scheme of LR enhancement factor formulas (5), (6). With this information, the σ_{ext} profiles are retrieved by the method of section 3.4.2. We then studied the relative biases between the parameterized σ_{ext} profiles and the retrieved σ_{ext} profiles by using the new method.

Different kinds of aerosol PNSD, AOD, aerosol hygroscopicity and RH profiles are used in the simulations. The realtive bias are statistically studied and summarized. The values listed in Table 1 are the mean relative biases under different PNSD conditions. From Table 1, we can see that all of the relative bias is within the range of 13% for different PNSD, AOD, aerosol hygroscopicity and RH profiles. This indicates that the algorithm of using the mean LR enhancement factor parameterization scheme is feasible and can decrease the bias of the retrieved elastic-backscatter lidar data significantly.

4.4 Retrieving the real-time measurement elastic-backscatter lidar signals

MPL data and AERONET data are employed to validate the algorithm of retrieving the elastic-backscatter lidar data on the day of 5 July 2016. After quality control of data processing, elastic-backscatter lidar data is retrieved by using both a constant LR profile method and a parameterized variable LR profile method. Details of retrieving the MPL signals and the auxiliary information are shown in fig.S5. Fig. 6 gives the retrieved σ_{ext} profiles ~~using~~ two ~~methods of~~ local time 13:00 (a) and 14:30 (b).

Fig. 6(a) is a typical case of the retrieved σ_{ext} profiles under high values of both RH and AOD conditions. The retrieved σ_{ext} profiles by using the constant LR profile method and variable LR profile method show almost the same properties as the simulations. The relative bias reaches a value of 39.3% at an altitude of 1.57 km. These differences of retrieved σ_{ext} profiles may lead to a significant bias of estimating the mixed layer height and have significant impact on radiative energy distribution in the vertical direction. Fig. 6(b) shows the retrieved σ_{ext} profiles of different structures from the same elastic-backscatter lidar data. The retrieved σ_{ext} by using variable LR profile method increases with height within the mixed layer. However, the retrieved σ_{ext} by using constant LR profile decreases slightly with height within the mixed layer.

5 Conclusions

The influence of aerosol hygroscopic growth on LR is evaluated by using Mie scattering theory. Datasets used as input to Mie theory model come from the Hachi Campaign field measurements and these datasets can be used as a good representation of the continental aerosols. Results show that LR in the NCP mainly ranges from 30 to 90 sr, which is consistent with literature values of continental aerosols. LR could be enhanced significantly under high RH conditions, with a mean factor of 2.2 at 92% RH.

RH in the mixed layer in the NCP is frequently observed to be higher than 90%. Under these conditions, large variation of LR in the vertical direction exists. This leads to significant bias of retrieved σ_{ext} profile due to a constant LR profile currently used to retrieve the elastic-backscatter lidar signals. The relative bias of the retrieved σ_{ext} profiles between the constant LR profile method and the variable LR profile method can reach up to 40% under high RH conditions ~~and the retrieved σ_{ext} profile structure can be different under low RH conditions~~.

Sensitivity studies ~~are~~ carried out to test the bias of retrieved σ_{ext} profiles. The bias increases linearly with RH at low RH but increases strongly at high RH. PNSD can lead to 10% standard deviation of the bias. Maximum bias happens under the conditions of both high AOD and RH that frequently happen in the NCP. The influence of aerosol hygroscopic growth on LR should be taken into consideration when retrieving the elastic-backscatter lidar data in the NCP.

A new algorithm accounting for the aerosol hygroscopic growth is proposed to retrieve the elastic-backscatter lidar data. A scheme of LR enhancement factor parameterization is introduced in this algorithm. The bias of retrieved σ_{ext} profiles by using this algorithm can be constrained within 13%. Real-time measurement of MPL data is employed to validate the algorithm and the results show good consistency with the simulations.

This research will advance our understanding of the influence of aerosol hygroscopic growth on LR and help to improve the retrieval of σ_{ext} profile from elastic-backscatter lidar signals.

Acknowledgments

This work is supported by the National Natural Science Foundation of China (41590872, 41375134).

References

Ackermann, J. (1998) The Extinction-to-Backscatter Ratio of Tropospheric Aerosol: A Numerical Study. Journal of Atmospheric and Oceanic Technology 15, 1043-1050.

Anderson, T.L., Anderson, T.L. (2003) Variability of aerosol optical properties derived from in situ aircraft measurements during ACE-Asia. Journal of Geophysical Research 108, ACE-15-11-ACE 15-19.

Anderson, T.L., Masonis, S.J., Covert, D.S., Charlson, R.J., Rood, M.J. (2000) In situ measurement of the aerosol extinction-to-backscatter ratio at a polluted continental site. Journal of Geophysical Research: Atmospheres 105, 26907-26915.

Andreae, M.O., Crutzen, P.J. (1997) Atmospheric Aerosols: Biogeochemical Sources and Role in Atmospheric Chemistry. Science 276, 1052-1058.

Ansmann, A., Wagner, F., Althausen, D., Müller, D., Herber, A., Wandinger, U. (2001) European pollution outbreaks during ACE 2: Lofted aerosol plumes observed with Raman lidar at the Portuguese coast. Journal of Geophysical Research Atmospheres 106, 20725–20733.

Ansmann, A., Wagner, F., Müller, D., Althausen, D., Herber, A., von Hoyningen-Huene, W., Wandinger, U. (2002) European pollution outbreaks during ACE 2: Optical particle properties inferred from multiwavelength lidar and star-Sun photometry. Journal of Geophysical Research: Atmospheres 107, AAC 8-1-AAC 8-14.

Bian, J., Chen, H., ouml, mel, H., Duan, Y. (2011) Intercomparison of humidity and temperature sensors: GTS1, Vaisala RS80, and CFH. Advances in atmospheric sciences 28, 139-146.

Bohren, C.F., Huffman, D.R., (2007) Absorption and Scattering by an Arbitrary Particle, Absorption and Scattering of Light by Small Particles. Wiley-VCH Verlag GmbH, pp. 57-81.

Chaikovsky, A., Dubovik, O., Holben, B., Bril, A., Goloub, P., Tanre, D., Pappalardo, G., Wandinger, U., Chaikovskaya, L., Denisov, S., Grudo, J., Lopatin, A., Karol, Y., Lapyonok, T., Amiridis, V., Ansmann, A., Apituley, A., Allados-Arboledas, L., Binietoglou, I., Boselli, A., D'Amico, G., Freudenthaler, V., Giles, D., Jose Granados-Munoz, M., Kokkalis, P., Nicolae, D., Oshchepkov, S., Papayannis, A., Perrone, M.R., Pietruczuk, A., Rocadenbosch, F., Sicard, M., Slutsker, I., Talianu, C., De Tomasi, F., Tsekeri, A., Wagner, J., Wang, X. (2016) Lidar-Radiometer Inversion Code (LIRIC) for the retrieval of vertical aerosol properties from combined lidar/radiometer data: development and distribution in EARLINET. Atmospheric Measurement Techniques 9, 1181-1205.

Chen, J., Zhao, C.S., Ma, N., Liu, P.F., Göbel, T., Hallbauer, E., Deng, Z.Z., Ran, L., Xu, W.Y., Liang, Z., Liu, H.J., Yan, P., Zhou, X.J., Wiedensohler, A. (2012) A parameterization of low visibilities for hazy days in the North China Plain. Atmos. Chem. Phys. 12, 4935-4950.

Chen, J., Zhao, C.S., Ma, N., Yan, P. (2014) Aerosol hygroscopicity parameter derived from the light scattering enhancement factor measurements in the North China Plain. Atmos. Chem. Phys. 14, 8105-8118.

Fernald, F.G. (1984) Analysis of atmospheric lidar observations: some comments. Applied Optics 23, 652-653.

Fernald, F.G., Herman, B.M., Reagan, J.A. (1972) Determination of Aerosol Height Distributions by Lidar. Journal of Applied Meteorology 11, 482-489.

Ferrare, R.A., Melfi, S.H., Whiteman, D.N., Evans, K.D., Poellot, M., Kaufman, Y.J. (1998) Raman lidar measurements of aerosol extinction and backscattering: 2. Derivation of aerosol real refractive index, single-scattering albedo, and humidification factor using Raman lidar and aircraft size distribution measurements. Journal of Geophysical Research: Atmospheres 103, 19673-19689.

Ferrare, R.A., Turner, D.D., Brasseur, L.H., Feltz, W.F., Dubovik, O., Tooman, T.P. (2001) Raman lidar measurements of the aerosol extinction-to-backscatter ratio over the Southern Great Plains. Journal of Geophysical Research: Atmospheres 106, 20333-20347.

Ferrero, L., Mocnik, G., Ferrini, B.S., Perrone, M.G., Sangiorgi, G., Bolzacchini, E. (2011) Vertical profiles of aerosol absorption coefficient from micro-Aethalometer data and Mie calculation over Milan. Science of the Total Environment 409, 2824-2837.

Ferrero, L., Perrone, M.G., Petraccone, S., Sangiorgi, G., Ferrini, B.S., Lo Porto, C., Lazzati, Z., Cocchi, D., Bruno, F., Greco, F., Riccio, A., Bolzacchini, E. (2010) Vertically-resolved particle size distribution within and above the mixing layer over the Milan metropolitan area. Atmospheric Chemistry and Physics 10, 3915-3932.

Gasteiger, J., Groß, S., Sauer, D., Haarig, M., Ansmann, A., Weinzierl, B. (2017) Particle settling and vertical mixing in the Saharan Air Layer as seen from an integrated model, lidar, and in situ perspective. Atmospheric Chemistry and Physics 17, 297-311.

He, Q.S., Li, C.C., Mao, J.T., Lau, A.K.H., Li, P.R. (2006) A study on the aerosol extinction-to-backscatter ratio with combination of micro-pulse LIDAR and MODIS over Hong Kong. Atmospheric Chemistry and Physics 6, 3243-3256.

Klett, J.D. (1981) Stable analytical inversion solution for processing lidar returns. Applied Optics 20, 211-220.

Klett, J.D. (1985) Lidar inversion with variable backscatter/extinction ratios. Applied Optics 24, 1638-1643.

Kuang, Y., Zhao, C.S., Tao, J.C., Bian, Y.X., Ma, N. (2016) Impact of aerosol hygroscopic growth on the direct aerosol radiative effect in summer on North China Plain. Atmospheric Environment 147, 224-233.

Kuang, Y., Zhao, C.S., Tao, J.C., Ma, N. (2015) Diurnal variations of aerosol optical properties in the North China Plain and their influences on the estimates of direct aerosol radiative effect. Atmos. Chem. Phys. 15, 5761-5772.

Liu, H.J., Zhao, C.S., Nekat, B., Ma, N., Wiedensohler, A., van Pinxteren, D., Spindler, G., Müller, K., Herrmann, H. (2014) Aerosol hygroscopicity derived from size-segregated chemical composition and its parameterization in the North China Plain. Atmospheric Chemistry and Physics 14, 2525-2539.

Liu, P., Zhao, C., Zhang, Q., Deng, Z., Huang, M., Xincheng, M.A., Tie, X. (2009) Aircraft study of aerosol vertical distributions over Beijing and their optical properties. Tellus Series B-chemical & Physical Meteorology 61, 756–767.

Liu, P.F., Zhao, C.S., Göbel, T., Hallbauer, E., Nowak, A., Ran, L., Xu, W.Y., Deng, Z.Z., Ma, N., Mildenberger, K., Henning, S., Stratmann, F., Wiedensohler, A. (2011) Hygroscopic properties of aerosol particles at high relative humidity and their diurnal variations in the North China Plain. Atmos. Chem. Phys. 11, 3479-3494.

Ma, N., Zhao, C.S., Müller, T., Cheng, Y.F., Liu, P.F., Deng, Z.Z., Xu, W.Y., Ran, L., Nekat, B., van Pinxteren, D., Gnauk, T., Müller, K., Herrmann, H., Yan, P., Zhou, X.J., Wiedensohler, A. (2012) A new method to determine the mixing state of light absorbing carbonaceous using the measured aerosol optical properties and number size distributions. Atmos. Chem. Phys. 12, 2381-2397.

Ma, N., Zhao, C.S., Nowak, A., Müller, T., Pfeifer, S., Cheng, Y.F., Deng, Z.Z., Liu, P.F., Xu, W.Y., Ran, L., Yan, P., Göbel, T., Hallbauer, E., Mildenberger, K., Henning, S., Yu, J., Chen, L.L., Zhou, X.J., Stratmann, F., Wiedensohler, A. (2011) Aerosol optical properties in the North China Plain during HaChi campaign: an in-situ optical closure study. Atmos. Chem. Phys. 11, 5959-5973.

Pappalardo, G., Amodeo, A., Mona, L., Pandolfi, M., Pergola, N., Cuomo, V. (2004a) Raman lidar observations of aerosol emitted during the 2002 Etna eruption. Geophysical Research Letters 31, 179-211.

Pappalardo, G., Amodeo, A., Pandolfi, M., Wandinger, U., Ansmann, A., Bösenberg, J., Matthias, V., Amiridis, V., De Tomasi, F., Frioud, M., Iarlori, M., Komguem, L., Papayannis, A., Rocadenbosch, F., Wang, X. (2004b) Aerosol lidar intercomparison in the framework of the EARLINET project. 3. Ramanlidar algorithm for aerosol extinction, backscatter, and lidar ratio. Applied Optics 43, 5370-5385.

Petters, M.D., Kreidenweis, S.M. (2007) A single parameter representation of hygroscopic growth and cloud condensation nucleus activity. Atmos. Chem. Phys. 7, 1961-1971.

Pietruczuk, A., Podgórski, J., (2009) The lidar ratio derived from sun-photometer measurements at Belsk Geophysical Observatory, Acta Geophysica, p. 476.

Pietruczuk, A., Podgorski, J. (2009) The lidar ratio derived from sun-photometer measurements at Belsk Geophysical Observatory. Acta Geophysica 57, 476-493.

Ran, L., Deng, Z., Xu, X., Yan, P., Lin, W., Wang, Y., Tian, P., Wang, P., Pan, W., Lu, D. (2016) Vertical profiles of black carbon measured by a micro-aethalometer in summer in the North China Plain. Atmospheric Chemistry and Physics 16, 10441-10454.

Rosati, B., Herrmann, E., Bucci, S., Fierli, F., Cairo, F., Gysel, M., Tillmann, R., Größ, J., Gobbi, G.P., Di Liberto, L., Di Donfrancesco, G., Wiedensohler, A., Weingartner, E., Virtanen, A., Mentel, T.F., Baltensperger, U. (2016) Studying the vertical aerosol extinction coefficient by comparing in situ airborne data and elastic backscatter lidar. Atmospheric Chemistry and Physics 16, 4539-4554.

Salemink, H.W.M., Schotanus, P., Bergwerff, J.B. (1984) Quantitative lidar at 532 nm for vertical extinction profiles and the effect of relative humidity. Applied Physics B 34, 187-189.

She, C.Y., Alvarez, R.J., Caldwell, L.M., Krueger, D.A. (1992) High-spectral-resolution Rayleigh–Mie lidar measurement ofaerosol and atmospheric profiles. Optics Letters 17, 541-543.

Shipley, S.T., Tracy, D.H., Eloranta, E.W., Trauger, J.T., Sroga, J.T., Roesler, F.L., Weinman, J.A. (1983) High spectral resolution lidar to measure optical scattering properties of atmospheric aerosols. 1: Theory and instrumentation. Applied Optics 22, 3716-3724.

Sroga, J.T., Eloranta, E.W., Shipley, S.T., Roesler, F.L., Tryon, P.J. (1983) High spectral resolution lidar to measure optical scattering properties of atmospheric aerosols. 2: Calibration and data analysis. Applied Optics 22, 3725-3732.

Sušnik, A., Holder, H., Eichinger, W. (2014) A Minimum Variance Method for Lidar Signal Inversion. Journal of Atmospheric and Oceanic Technology 31, 468-473.

Wex, H., Neususs, C., Wendisch, M., Stratmann, F., Koziar, C., Keil, A., Wiedensohler, A., Ebert, M. (2002) Particle scattering, backscattering, and absorption coefficients: An in situ closure and sensitivity study. Journal Of Geophysical Research-Atmospheres 107.

Xu, W.Y., Zhao, C.S., Ran, L., Deng, Z.Z., Liu, P.F., Ma, N., Lin, W.L., Xu, X.B., Yan, P., He, X., Yu, J., Liang, W.D., Chen, L.L. (2011) Characteristics of pollutants and their correlation to meteorological conditions at a suburban site in the North China Plain. Atmos. Chem. Phys. 11, 4353-4369.

Table 1. Relative difference (%) between the σ_{ext} profiles by using the proposed new method and the parameterized σ_{ext} profiles under different AOD and RH profile conditions

		AOD							
		0.2	**0.4**	**0.6**	**0.8**	**1.0**	**1.2**	**1.4**	**1.6**
RH profile	**P60-70**	**6**	**9**	**11**	**13**	**8**	**8**	**8**	**9**
	P70-80	**7**	**7**	**9**	**12**	**7**	**6**	**7**	**8**
	P80-90	**8**	**5**	**4**	**11**	**6**	**5**	**5**	**6**
	P90-95	**9**	**6**	**6**	**9**	**13**	**7**	**7**	**9**

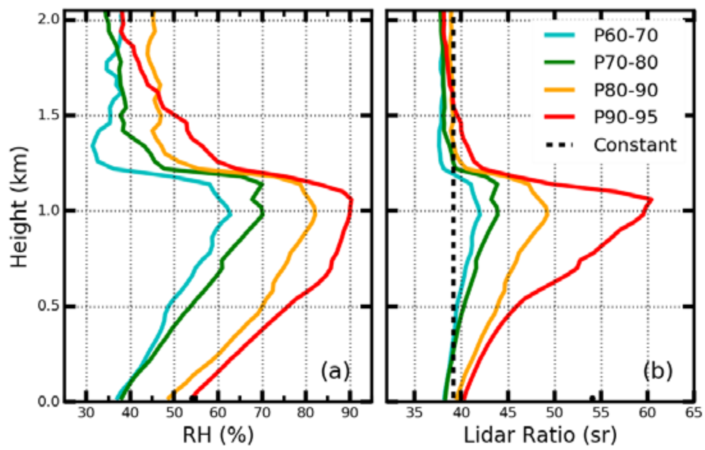

Figure 1. (a) Four kinds of RH profiles P60-70, P70-80, P80-90, and P90-95; (b) calculated LR profiles from the corresponding RH profiles of (a). Dotted black line is one of the constant LR profiles that are used to retrieve the MPL signals.

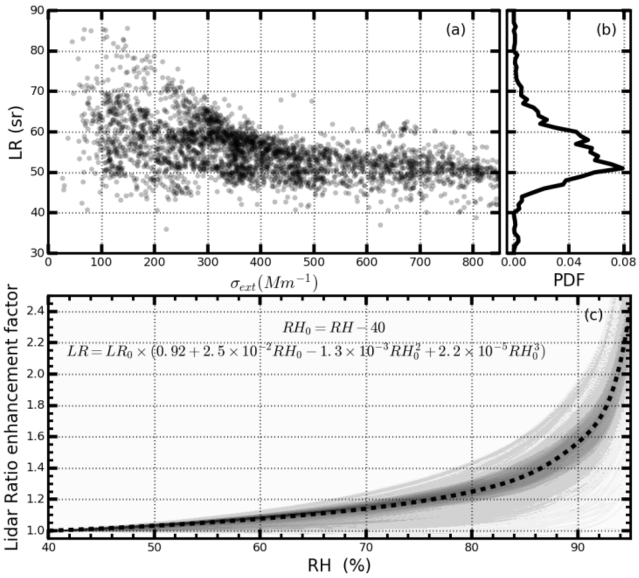

Figure 2. LR distribution and LR enhancement factor during Hachi campaign. (a) LR distribution under different polluted conditions. (b) Probability distribution of the LR. (c) Enhancement factor of the LR. Dotted line is the mean fit LR enhancement factor.

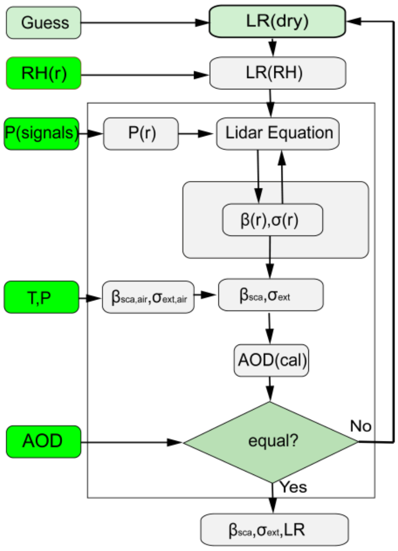

Figure 3. Schematic diagram of retrieving the σ_{ext} profile. The input variables are displayed in green background.

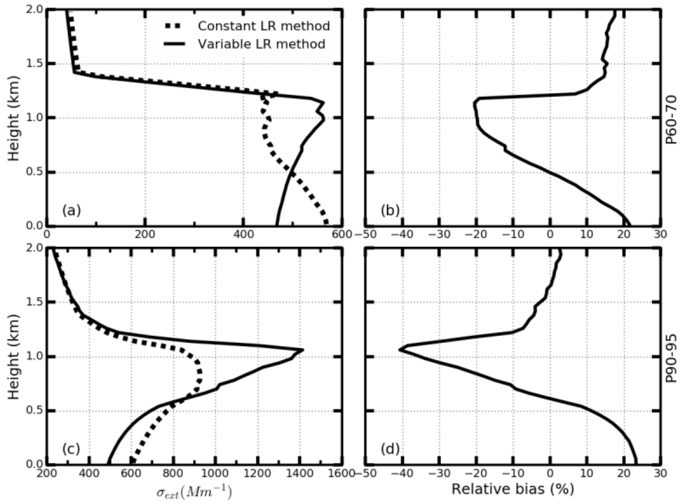

Figure 4. (a) Retrieved σ_{aero} profiles using constant LR profile method (dotted line) and variable LR profile method (solid line) from simulated lidar signals. (b) The relative bias of the retrieved σ_{aero} profile using two different methods. (c),(d）are the same as (a), (b) respectively. The LR signals of panel (a) results form P70-80 RH profile, and LR signals of panel (b) results from P90-95 RH profile

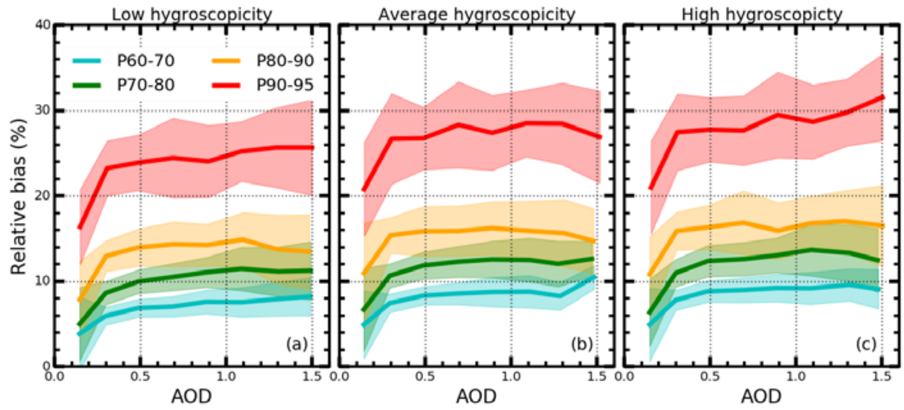

Figure 5. Relative bias of the retrieved σ_{ext} under different AOD, PNSD, and hygroscopicity and RH profiles conditions. Different colors represent different RH profile. Panel (a) is derived from the low hygroscopicity. Panel (b) results from the mean hygroscopicity. Panel (c) is for high hygroscopicity.

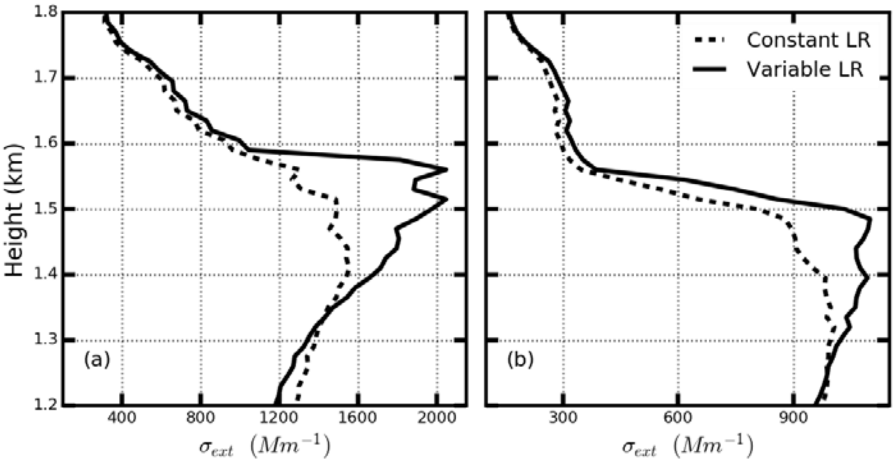

Figure 6. Retrieved σ_{ext} profiles from field measurement MPL signals at (a) 13:00 and (b) 14:30 on July 5, 2016. Dotted line represents the retrieved σ_{ext} profiles using constant LR profile method. Solid line represents the retrieved σ_{ext} profiles using variable LR profile method.